Mon. Not. R. Astron. Soc. **000**, 000–000 (0000) Printed 17 July 2000 (MN LATEX style file v1.4)

Peculiar velocities of galaxies and clusters

Ravi K. Sheth[1] & Antonaldo Diaferio[2]
[1] *NASA/Fermilab Astrophysics Group, Batavia, IL 60510-0500*
[2] *Dipartimento di Fisica Generale "Amedeo Avogadro", Università di Torino, Italy*
Email: sheth@fnal.gov, diaferio@ph.unito.it

2000 June 30

ABSTRACT
We present a simple model for the shape of the distribution function of galaxy peculiar velocities. We show how both nonlinear and linear theory terms combine to produce a distribution which has an approximately Gaussian core with exponential wings. The model is easily extended to study how the statistic depends on the type of particle used to trace the velocity field (dark matter particles, dark matter haloes, galaxies), and on the density of the environment in which the test particles are. Comparisons with simulations suggest that our model is accurate. We also show that the evolution of the peculiar velocities depends on the local, rather than the global density. Since clusters populate denser regions on average, using cluster velocities with the linear theory scaling may lead to an overestimate of the global value of Ω_0. Conversely, using linear theory with the global value of Ω_0 to scale cluster velocities from the initial to the present time results in an underestimate of their true velocities. In general, however, the directions of motions of haloes are rather well described by linear theory. Our results help to simplify models of redshift-space distortions considerably.

Key words: galaxies: clustering – cosmology: theory – dark matter.

1 INTRODUCTION

The gravitational evolution of the density field in an expanding Universe modifies the shape of the distribution function $f(v)\,\mathrm{d}v$ of the peculiar velocity field. Because of the action of gravity, the dark matter distribution at the present time is certainly not an ideal gas, so it should come as no surprise that the present-day distribution of velocities is quite different from the Maxwell-Boltzmann. Although it has been known for some time that the variance of this distribution is sensitive to the background cosmology, the first detailed model of how and why the shape of this distribution differs from a Maxwell-Boltzmann was discussed by Saslaw et al. (1990).

Here we present a model for the shape of the peculiar velocity distribution $f(v)\,\mathrm{d}v$ which captures the essence of the evolution driven by gravitational instability. Our model explicitly includes the type of particle tracing the velocity field: dark matter particles, galaxies, or galaxy clusters. This feature of the model is crucial because galaxies and clusters trace the underlying distribution of dark matter differently and measurements of $f(v)\,\mathrm{d}v$, in which either galaxies or galaxy clusters are used as trace particles (e.g., the Mark III sample of Willick et al. 1997, the SFI sample of Giovanelli et al. 1998 and Haynes et al. 1999a,b, and the ENEAR sample of da Costa et al. 2000) are widely used to constrain cosmological models.

Section 2 describes our model. In essence, we write the motion of a dark matter particle as the sum of two terms, one of which evolves according to linear theory, and another which is inherently nonlinear. Section 2.1 shows that this split provides a good approximation to what happens in N-body simulations, and Section 2.2 shows that our model provides a good description of the shape of $f(v)$ for the dark matter. Section 2.3 describes how the model can be used to study the dependence of the shape of $f(v)$ on the local density, and Section 2.6 shows how and why the distribution of halo velocities is different from that of dark matter particles. This leads, in Section 2.6, to a discussion of how the model can be extended to provide predictions for how $f(v)$ depends on galaxy type.

In addition to studying velocities at the present time, we also study how velocities evolve from some early time to the present. Section 3 argues that the evolution of halo speeds should show some dependence on local density, and presents results from simulations showing that this actually does happen. We also study how the direction of motion of trace particles evolves. We show that linear theory describes the directions in which dark matter particles are moving today rather badly, but the directions of halo motions very well, and discuss some useful consequences of this fact. We summarize our findings in Section 4.

2 THE DISTRIBUTION FUNCTION OF VELOCITIES

The key assumptions of this model are similar to those discussed by Sheth (1996) and Diaferio & Geller (1996) in their discussions of the distribution of pairwise velocities. Indeed, the model described below is essentially the same as that discussed in the second half of Sheth (1996), where a detailed discussion of the significant differences between our approach and that of Saslaw et al. (1990) can also be found. The final subsection discusses how the model can be extended to describe what happens when dark matter haloes or galaxies, rather than dark matter particles, are used to construct the statistic.

2.1 Assumptions

All dark matter particles are assumed to be in approximately spherical, virialized haloes. The velocity of a dark matter particle is assumed to depend on two variables: the mass of the halo in which it is, and the local density in which the parent halo is. Although the local density is, in principle, a function of smoothing scale, we show below that if this scale is chosen so that it typically contains many halos, then our results are relatively insensitive to the exact choice. Let $p(v|m,\delta)\,{\rm d}v$ denote the probability that a particle in a halo of mass m which is in a region within which the average density is $(1+\delta)$ times the background density, has velocity in the range ${\rm d}v$ about v. Then the distribution of interest is given by summing up the various $p(v|m,\delta)$ distributions, weighting by the fraction of particles which are in haloes of mass m in regions of overdensity δ:

$$f(v) = \frac{\int {\rm d}\delta\, p(\delta) \int {\rm d}m\, m\, n(m|\delta)\, p(v|m,\delta)}{\int {\rm d}\delta\, p(\delta) \int {\rm d}m\, m\, n(m|\delta)}, \qquad (1)$$

where $n(m|\delta)\,{\rm d}m$ is the number density of haloes that have mass in the range ${\rm d}m$ about m and are in regions within which the average density is δ, and $p(\delta)\,{\rm d}\delta$ is the fraction of regions which have density in the range ${\rm d}\delta$ about δ. The weighting by m reflects the fact that the number of dark matter particles in a halo is supposed to be proportional to the halo mass. This expression holds both for the size of the velocity vector itself, which we will often call the speed, as well as for the individual velocity components.

If we rearrange the order of the integrals in the denominator, and then integrate over δ, then what remains is $\int {\rm d}m\, m\, n(m)$, where $n(m)$ is the average density of haloes of mass m averaged over all environments, so it is often called the universal halo mass function. Because all particles are assumed to be in haloes, this universal mass function is normalized so that $\int {\rm d}m\, m\, n(m)$ equals the background density $\bar\rho$.

To proceed, we need estimates of $n(m|\delta)$ and of $p(v|m,\delta)$. In what follows, we will study the case of clustering from Gaussian initial conditions in detail. If the initial conditions are non-Gaussian, $n(m|\delta)$ and $p(v|m,\delta)$ are of course different from what we use, but our equation (1) is still valid.

For hierarchical clustering from Gaussian initial conditions, a good a pproximation to the universal number density $n(m)$ of haloes of mass m is given, for arbitrary power-spectra, cosmology and times, by Press & Schechter (1974). In what follows we will use the simple modification to this formula provided by Sheth & Tormen (1999) which is considerably more accurate:

$$n(m) = \frac{A\bar\rho}{m^2}\left(1+\frac{1}{(a\nu^2)^p}\right)\sqrt{\frac{a\nu^2}{2\pi}}\exp\left(\frac{-a\nu^2}{2}\right)\frac{{\rm d}\ln\nu^2}{{\rm d}\ln m}, \qquad (2)$$

where $\bar\rho$ is the average background density, $A = 0.322$, $a = 0.707$, $p = 0.3$ and $\nu = \delta_{\rm c}/\sigma(m)$ with $\delta_{\rm c} \approx 1.686$ and $\sigma^2(m)$ represents the variance in the initial density field, when smoothed on the scale $R = (3m/4\pi\bar\rho)^{1/3}$, extrapolated to the present time using linear theory. The Press-Schechter formula has $A = 0.5$, $a = 1$ and $p = 0$. Sheth, Mo & Tormen (2000) argue that whereas the Press-Schechter formula is associated with models in which haloes form from a spherical collapse, this more accurate formula is associated with ellipsoidal collapse.

What we really need is $n(m|\delta)$. Unfortunately, the simplest approximation to this distribution is not accurate (Lemson & Kauffmann 1999; Sheth & Lemson 1999): $n(m|\delta) \neq (1+\delta)\, n(m)$. However, a good approximation to the actual distribution can be computed following the work of Mo & White (1996):

$$n(m|\delta) \approx \Big[1 + b(m)\delta\Big]\, n(m), \qquad (3)$$

where $b(m)$ depends on the halo mass (Mo & White 1996) and on the shape of $n(m)$ (Sheth & Tormen 1999). This approximation is accurate provided that δ is defined by smoothing the density field on scales that are sufficiently large that a randomly placed cell contains many haloes. Equations (10) and (11) in Sheth & Tormen (1999) give the $b(m)$ relation associated with the $n(m)$ distribution we use in this paper (our equation 2). For massive haloes, $b(m)$ increases with m, so the ratio of the number of massive to less massive haloes is larger in dense regions than in underdense regions. The exact form of the predicted dependence on δ is slightly more complicated than the simple approximation shown above, and is in reasonably good agreement with simulations (Sheth & Tormen 2000). When computing the model predictions which follow, we actually use the exact formula for $n(m|\delta)$, rather than the simpler approximation shown above.

We now turn to the other term, $p(v|m,\delta)$. To model $p(v|m,\delta)$ we will assume that the velocity of any given dark matter particle is the sum of two terms,

$$v = v_{\rm vir} + v_{\rm halo}\,: \qquad (4)$$

the first is due to the velocity of the particle about the centre of mass of its parent halo, and the second is due to the motion of the centre of mass of the parent. We will assume that each of these terms has a dispersion which depends on both halo mass and on the local environment, so that

$$\sigma^2(m,\delta) = \sigma^2_{\rm vir}(m,\delta) + \sigma^2_{\rm halo}(m,\delta). \qquad (5)$$

The assumption that the virial motions within a halo are independent of the halo's environment, is probably reasonably accurate. It is not clear that the same is true for the halo speeds. Indeed, in the next section we will show that haloes in dense regions move faster than those in underdense regions. It will turn out, however, that the fraction of regions in which $\sigma^2_{\rm halo}(m,\delta)$ is significantly different from $\sigma^2_{\rm halo}(m,0)$ is quite small. This means that neglecting the

density dependence of the second term should be a reasonable approximation.

In what follows, we will assume that the dispersion depends on the mass of the parent halo, but not the local density: $\sigma^2(m,\delta) = \sigma^2(m)$. In fact, we will make the even stronger assumption that what is true of the second moment is also true of the distribution itself: $p(v|m,\delta) = p(v|m)$. In this case, we can rearrange the order of the integrals in the numerator of equation (1), and then integrate over δ to get

$$f(v) = \int \mathrm{d}m\, m\, \frac{n(m)}{\bar{\rho}}\, p(v|m), \qquad (6)$$

where we have used the fact that the integral over δ gives the universal mass function, and the integral of m times the universal mass function over all m gives the average density. To proceed, we need a model for the actual shape of $p(v|m)$. Since v is the sum of two random variates, we study each in turn.

Consider the first term, $v_{\rm vir}$. We will assume that virialized haloes are isothermal spheres, so that the distribution of velocities within them is Maxwellian. This is in reasonable agreement with simulations. Accounting for the fact that haloes really have more complicated density and velocity profiles is a detail which complicates the analysis, but not the logic of our argument. The main reason for this is that in the isothermal sphere model, the velocity dispersion of particles within the halo is independent of where they are within the halo.

What is the dispersion of this Maxwellian? At any given time, the average density of a virialized halo is approximately independent of the halo mass. This means that the mass m and size r of a halo are related: $m/(4\pi r^3/3)$ is a constant, typically equal to about 200 times the critical density at that time. This, with the virial requirement that $m/r \propto \sigma^2_{\rm vir}$, implies that the dispersion of the Maxwellian depends on halo mass: $\sigma^2_{\rm vir}(m,a) \propto m^{2/3}$. The constant of proportionality depends on time a and cosmology, and on the exact shape of the density profile of the halo. We will use the relations provided by Bryan & Norman (1998) to set this constant:

$$\sigma_{\rm vir}(m,a) = 476\, g_\sigma\, (\Delta_{\rm nl}\, E^2)^{1/6} \left(\frac{m}{10^{15} M_\odot/h}\right)^{1/3} \frac{\rm km}{\rm s}, \qquad (7)$$

where $g_\sigma = 0.9$, $\Delta_{\rm nl} = 18\pi^2 + 60x - 32x^2$ with $x = \Omega(a) - 1$, $\Omega(a) = (\Omega_0/a^3)/E^2(a)$, $E^2(a) = \Omega_0/a^3 + \Omega_R/a^2 + \Omega_\Lambda$, $a = 1/(1+z)$, where z is the redshift, so $a = 1$ at the present, $\Omega_0(a)$ is the ratio of the energy density in matter to the critical density, and Ω_Λ denotes the corresponding ratio for the energy density associated with a cosmological constant. Fig. 18 below shows that we are safe in assuming that this virial term is independent of local environment.

We turn, therefore, to the second term, $v_{\rm halo}$. It will prove more convenient to first study halo speeds after averaging over all environments, before considering the speeds as a function of local density. (This parallels the order in which we presented the halo mass function and its dependence on density.) Consider a halo of size r at the present time. Because the initial density fluctuations were small, the particles in this halo must have been drained from a larger region R in the initial conditions: $R/r \approx \Delta_{\rm nl}^{1/3}$, where $\Delta_{\rm nl} \approx 200$ or so (see text following equation 7). This means, for example, that massive haloes were assembled from larger regions than less massive haloes. Suppose we compute the rms value of the initial velocities of all the particles which make up a given halo. If we do this for all the haloes of mass m, then this is similar to computing the rms velocity in linear theory, smoothed on the scale $R(m) \propto m^{1/3}$.

It is well known that the linear theory prediction for the evolution of velocities is more accurate than the linear theory prediction for the evolution of the density. Although linear theory provides a useful estimate of the initial rms velocities of patches in the initial conditions that become haloes at $z = 0$, Colberg et al. (2000) showed that it is more accurate to assume that the massive haloes are associated with peaks in the initial fluctuation field. Bardeen et al. (1986) showed that the linear theory rms velocity of regions which are peaks when smoothed on the scale $R(m)$ is slightly smaller than that of average regions of the same scale, and Colberg et al. showed that the peak estimate agrees with the initial rms velocities of the haloes in their simulations to within about 20% or so. Colberg et al. only studied the most massive objects in their simulations; in what follows, we will show that the linear theory rms velocities of peaks provides an accurate estimate of the initial rms velocities of haloes of all masses.

Since we are interested in the rms velocities of haloes at the present time (i.e., not in the initial conditions), we must know how these velocities evolve. Colberg et al. (2000) showed that scaling the rms velocities of peaks using the linear theory provided an underestimate of the actual growth of the rms velocities of the massive clusters in their simulations. They showed that this procedure provides velocities which are accurate to within 40% or so at $z = 0$. While this is good enough for the results presented in the first part of this section (we will discuss why shortly), many of the results to follow are sensitive to this difference. Therefore, Section 3 studies the reason for this underestimate.

To summarize: in what follows, we will assume that at the present time, the velocities of all haloes, not just the massive ones, are reasonably well described by extrapolating the velocities of peaks (smoothed on the relevant scale: $R \propto m^{1/3}$) using linear theory. For Gaussian initial conditions, this means that any given value of $v_{\rm halo}$ is drawn from a Maxwellian with dispersion $\sigma^2_{\rm halo}(m)$ given by:

$$\sigma_{\rm halo}(m) = H_0 \Omega_0^{0.6}\ \sigma_{-1}\ \sqrt{1 - \sigma_0^4/\sigma_1^2\sigma_{-1}^2}, \qquad (8)$$

where H_0 and Ω_0 are the Hubble constant and the density parameter at the present time,

$$\sigma_j^2(m) = \frac{1}{2\pi^2} \int \mathrm{d}k\ k^{2+2j}\, P(k)\, W^2[kR(m)],$$

and $W(x)$ is the Fourier transform of the smoothing window. For the TopHat in real space that we will use in the remainder of this paper, $W(x) = (3/x^3)\,[\sin(x) - x\,\cos(x)]$. Notice that the predicted rms velocity depends both on cosmology and on the shape of the power spectrum. The term under the square-root arises from the peak constraint—it tends to unity as m decreases: the peak constraint becomes irrelevant for the less massive (small R) objects.

We have found that

$$\sigma_{\rm halo}(m) = \frac{\sigma_{\rm fit}}{1 + (R/R_{\rm fit})^\eta} \qquad (9)$$

Model	Ω_0	h	σ_8	$\sigma_{\rm fit}$ (km/s)	$R_{\rm fit}$ (Mpc/h)	η
SCDM	1.0	0.5	0.60	513.9	1.20	0.87
OCDM	0.3	0.7	0.85	474.6	1.54	0.85
ΛCDM	0.3	0.7	0.90	414.7	1.54	0.85

Table 1. Model parameters

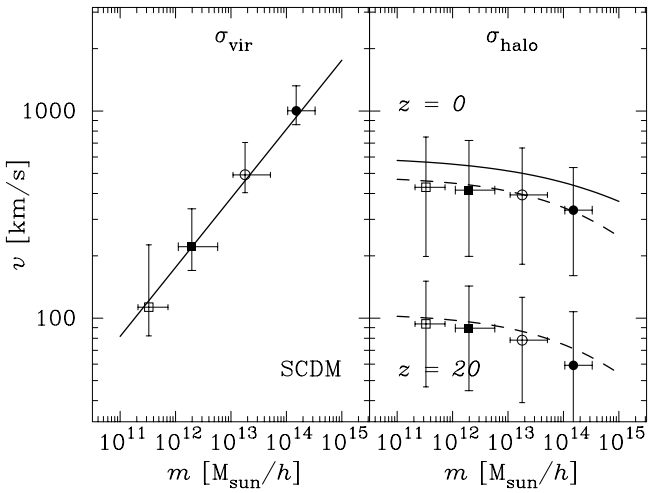

Figure 1. Dependence on halo mass of the nonlinear ($\sigma_{\rm vir}$) and linear theory ($\sigma_{\rm halo}$) terms in our model. Solid curves show the scaling we assume, and symbols show the corresponding quantities measured in the $z = 0$ output time of the SCDM GIF simulation. Error bars show the 90 percentile ranges in mass and velocity. Dashed curve in panel on right shows the expected scaling after accounting for the finite size of the simulation box. Symbols and curves in the bottom of the panel on the right show the predicted and actual velocities at $z = 20$.

provides a good fit to equation (8) in the CDM family of models; Table 1 gives the values of $\sigma_{\rm fit}$, $R_{\rm fit}$ and η for the three representative models we consider in this paper. With these values, the fit is better than about 2% for SCDM, and about 1% for ΛCDM, over the range $0.05 \leq R \leq 50$ Mpc/h.

Fig. 1 compares the dependence on mass we assume for our two terms with that measured in numerical simulations of clustering in an SCDM universe (see Kauffmann et al. 1999 for details of the GIF collaboration simulations). The symbols with error bars show the median and ninety percentile ranges in mass and velocity. Open squares, filled squares, open circles and filled circles show haloes which have 60-100, 100-10^3, 10^3-10^4 and 10^4-10^5 particles, respectively. There are two sets of symbols in the panel on the right. For the time being, we are only interested in the symbols in the upper half which show halo velocities at $z = 0$. The solid curves in the two panels show the scalings we assume.

Although the scaling of the virial term with mass is quite accurate, it appears that the extrapolated linear theory velocities are considerably in excess of the measurements in the simulations. This is almost entirely due to the finite size of the simulation box. The upper dashed curve shows the effect of using equation (8) to estimate the rms speeds of halos, after setting $P(k) = 0$ for $k < 2\pi/L$, where L is the box-size: $L = 85$ Mpc/h for SCDM and it is 141 Mpc/h for ΛCDM. Thus, the two panels show that our simple estimates of the two contributions to the variance of $p(v|m)$ are reasonably accurate.

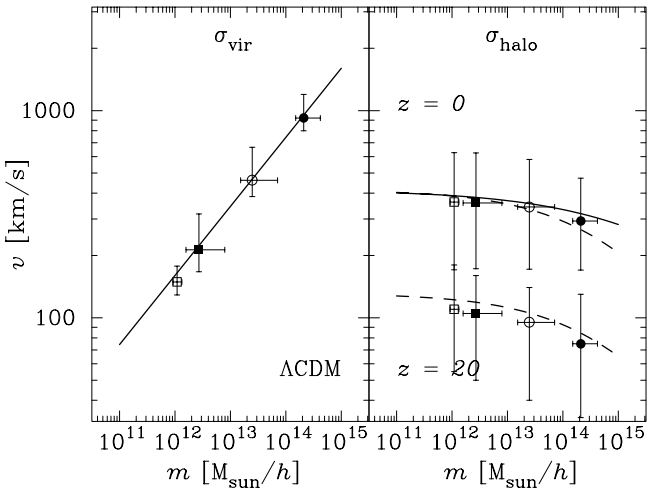

Figure 2. As for the previous Figure, but for ΛCDM. Since the simulation box is larger, finite size effects are less dramatic.

Fig. 2 shows a similar comparison between our model scalings and the GIF simulation of a ΛCDM cosmology. In this case, the simulation box is larger, so the finite box-size effects on the halo velocities are much less dramatic. Although the accuracy of the scaling of the virial term with mass is well known, the reasonably good agreement of the extrapolated linear theory peak velocities, over the entire mass range present in the simulations, is new.

Notice that the two terms scale differently with halo mass; indeed, to a first approximation, one might even argue that halo speeds are independent of halo mass. Since our model for the average halo speeds is really only accurate to within about 40% or so (e.g. Colberg et al. 2000 for the massive haloes), it is interesting to consider how much we expect our use of linear theory peak velocities, and our neglect of the possibility that the speeds may depend on environment, to influence the results which follow. In the ΛCDM model at small masses, the linear theory prediction is not affected by box size (the solid and dashed curves in the panel on the right are similar), and it provides a good description of the average halo speeds. It is at larger masses where the inaccuracy of linear theory may be problematic. Fortunately, Fig. 2 shows that $\sigma_{\rm halo}(m) < \sigma_{\rm vir}(m)$ for massive haloes. Since massive haloes have larger dispersions than less massive haloes, the large velocity tail of $f(v)$ is determined primarily by the nonlinear virial motions within massive haloes, rather than by the peculiar motions of the halo centres of mass. For this reason, the large velocity tails of $f(v)$, at least, are unlikely to be sensitive to inaccuracies in our treatment of halo velocities, or to our neglect of the possibility that halo speeds may depend on their environment.

We are finally in a position to specify our model for $p(v|m)$. Recall that the virial motions are Maxwellian, and that, for Gaussian initial density fluctuations, our linear peaks theory model of the halo motions means that they too are Maxwellian. Thus, in our model, each of the three cartesian components of the velocity of a dark matter particle in a clump of mass m is given by the sum of two Gaussian

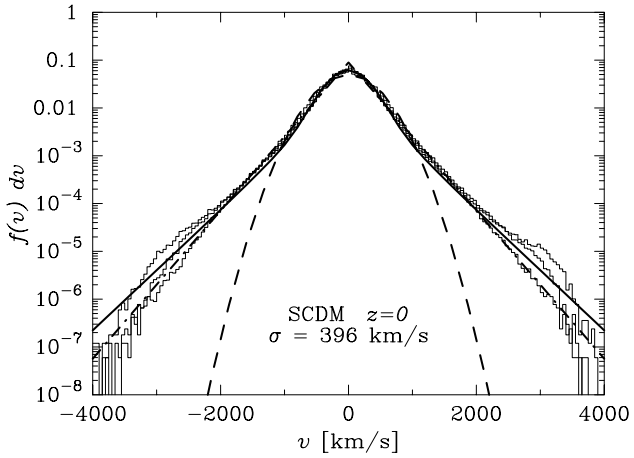

Figure 3. The distribution of one-dimensional peculiar velocities for dark matter particles in a SCDM cosmology. Histograms show the distribution of the three cartesian components measured in the GIF simulations. Dashed and dot-dashed curves show Gaussian and exponential distributions which have the same dispersion. The solid curve shows the distribution predicted by our model, after accounting for the finite size of the simulation box. The exponential wings are almost entirely due to virial motions within haloes.

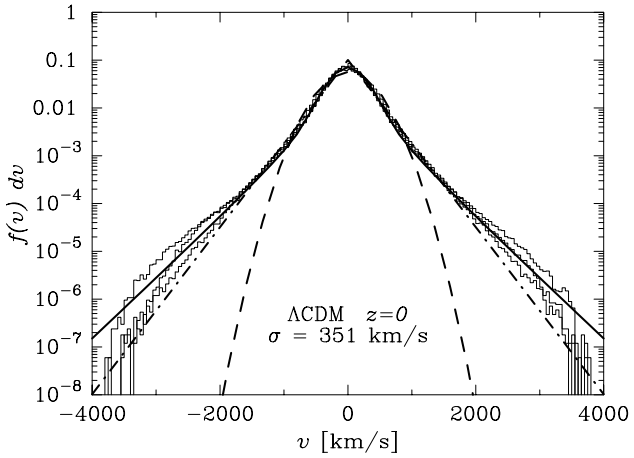

Figure 4. As for the previous Figure, but for ΛCDM.

distributed random variates, one with dispersion $\sigma^2_{\rm vir}(m)/3$ and the other with $\sigma^2_{\rm halo}(m)/3$. If we further assume that the motion around the clump centre is independent of the motion of the clump as a whole, so these two Gaussian variates are independent, then $p(v|m)$ is Maxwellian (equation 15 gives the exact shape) with a dispersion which is the sum of the individual dispersions (the sum in quadrature of equations 7 and 8). This model for $p(v|m)$ can be thought of as a simple way in which the contributions to the velocity distribution statistic are split up into a part that is due to nonlinear effects (the first term) and a part which follows from extrapolating linear theory to a later time (the second term).

Our model should be reasonably accurate even if the initial conditions were non-Gaussian. Of course, non-Gaussian initial conditions have different $n(m)$ and $n(m|\delta)$ distributions than the ones we use here, though they can be computed from the statistics of the density fluctuation field similarly to how they were computed in the Gaussian case (e.g. Lucchin & Matarrese 1988; Robinson & Baker 1999; Sheth 2000). Although the virial motions are likely to still be Maxwellian, the fact that the linear peak theory velocities studied above were Maxwellians is specific to Gaussian initial conditions. In general, $p(v|m,\delta)$ will likely be different from a Maxwellian, although again, in linear theory, it too can be computed from the statistics of the initial density field.

2.2 Dark matter particles

Having described our model assumptions, we are ready to compare our predictions with simulations. In practice, we are only likely to observe velocities along the line of sight. This means that we will eventually be interested in the distribution of $f(v)$ projected along the line of sight. Projection changes the Maxwellian $p(v|m)$ distributions into Gaussians:

$$p(v|m) = \frac{{\rm e}^{-[v/\sigma(m)]^2/2}}{\sqrt{2\pi\sigma^2(m)}}, \qquad (10)$$

where $\sigma^2(m)$ is one third of the sum in quadrature of equations (7) and (8). Figs. 3 and 4 show the one-dimensional $f(v)$ distribution for two representatives of the CDM family of models presented in Figs. 1 and 2. The histograms show the distribution measured in the GIF simulations. For comparison, the dashed and dot-dashed curves in each panel show Gaussians and exponential distributions which have the same dispersion. The solid curves show the distribution predicted by our simple model (equations 6, 2, and 10). Exponential wings, and a small $|v|$ core that is more Gaussian than exponential are a generic prediction of our model. The exponential wings are almost entirely due to nonlinear motions within massive haloes, so they are fairly insensitive to our assumptions about how fast these haloes move. We conclude that our model provides a reasonably good description of what actually happens in the simulations. It is worth emphasizing that $\sigma(m)$ in equation (10) is set by the cosmological model and the initial conditions. Thus, the second moments of the distributions in Figs.3 and 4 are not free parameters of our model. The agreement with simulations suggests that our simple treatment of nonlinear and linear contributions to the statistic, and our assumption that any dependence on local density can be neglected, are sufficiently accurate.

2.3 Dependence on local density

Kepner, Summers & Strauss (1997) argue that it may be useful to compute velocity statistics as functions of local density, where the local density is defined as the mass contained within some larger smoothing scale, divided by the volume of the larger scale. Kepner et al. were actually interested in the pairwise velocity distribution, rather than the single particle distribution function considered here, but, following Sheth (1996) and Diaferio & Geller (1996), our discussion below of $f(v|\delta)$ applies equally to the pairwise statistic in which they were interested. Our calculation of $f(v)$ is easily extended to provide a model of $f(v|\delta)$.

If we require that

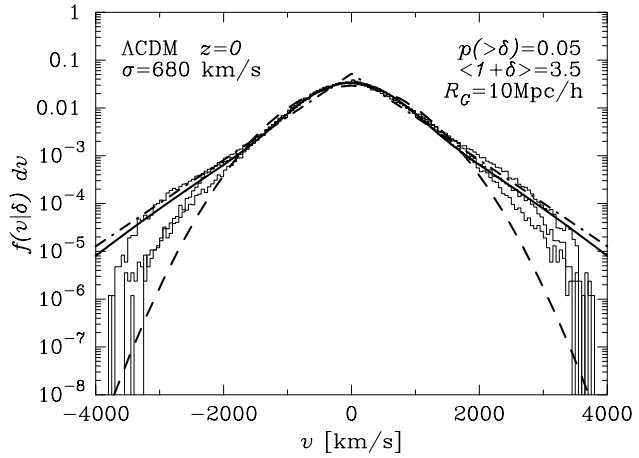

Figure 5. As for the previous Figure, but using only the particles which were in the densest regions of a ΛCDM model. The density was defined by smoothing the density (but not the velocities) with a Gaussian filter of size $R_{\rm G} = 10{\rm Mpc}/h$. Figure shows results for the densest 5% of the particles.

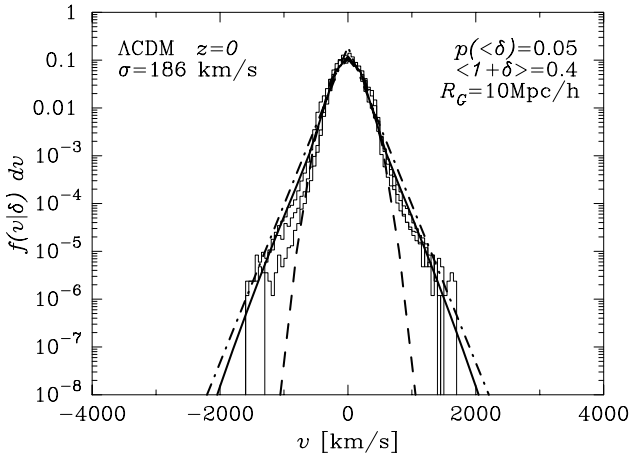

Figure 6. As for the previous Figure, but for underdense regions: the least dense 5% of the particles.

$$f(v) = \int f(v|\delta)\, p(\delta)\, {\rm d}\delta \qquad (11)$$

where $p(\delta)$ is the fraction of cells which have overdensity δ, and we have not written explicitly that both terms in the integrand depend on the smoothing scale used to define the local density, then equation (1) shows that the density-dependent statistic of interest in this section is

$$f(v|\delta) = \int p(v|m,\delta)\, \frac{m\, n(m|\delta)}{\bar\rho}\, {\rm d}m. \qquad (12)$$

In the context of our model, $f(v|\delta)$ may depend on local density either because the distribution of halo masses depends on local density or because the distribution of halo speeds depends on the local density, or both.

We have already discussed how the number density of haloes of mass m depends on δ (equation 3), We now turn to the other term, $p(v|m,\delta)$. Recall that the assumption that the virial term is independent of δ is accurate. If halo speeds are also independent of their environment, then $p(v|m,\delta)$ will be the same sum of two Gaussians that we used in the previous section: $p(v|m,\delta) = p(v|m)$. In other words, if halo speeds are independent of their surroundings, then $f(v|\delta)$ will differ from the global $f(v)$ simply because massive haloes, which have higher virial motions, occur predominantly in dense regions. Similarly, because less dense cells have fewer massive halos than average, the virial contribution in underdense cells is slightly lower than average. So, the rms velocity in less dense cells should be smaller than in denser cells.

Section 3 shows that, in fact, haloes in denser regions move faster than haloes in less dense regions. Although the shape of the distribution of the halo speeds remains approximately Gaussian, the dispersion depends on density. We incorporate this into our model by setting

$$p(v|m,\delta) = \frac{{\rm e}^{-[3v^2/\sigma^2(m,\delta)]/2}}{\sqrt{2\pi\sigma^2(m,\delta)/3}}, \qquad (13)$$

where

$$\sigma^2(m,\delta) = \sigma^2_{\rm vir}(m) + (1+\delta)^{2\mu}\, \sigma^2_{\rm halo}(m), \qquad (14)$$

and where the two σs are given in equations (7) and (8). As discussed in the next section, μ depends on the cell size on which δ was defined ($\mu = 0.6$ for the results which follow). In the previous subsection, we were able to neglect this dependence on δ because the fraction of regions in which the dispersion was significantly different from the average value was small. Here, because we are studying the distribution as a function of δ, we cannot ignore this dependence.

The histograms in Figs. 5 and 6 show the $f(v|\delta)$ distribution for the densest and least dense regions in the ΛCDM simulations. They were constructed by computing the density field on a 256^3 grid with the cloud-in-cell technique, and smoothing the density field using a Gaussian filter of scale $R_G = 10$ Mpc/h. Each particle was then assigned a density equal to that of the nearest grid point. The figures show the distribution of speeds for the densest and least dense 5% of the particles. The average overdensity of these particles is given in the top right hand corner of the two panels.

To compute the associated theory curves we must integrate over the probability $p(\delta)$ that a cell has overdensity δ. Since we simply wish to illustrate that our model can account for the striking differences between the two plots, we will show the result of simply using the value of the integrand at the mean value of the overdensity, rather than doing the integral exactly. To compute this representative overdensity, we must account for the fact that the theory requires the value of the density in a tophat filter whereas the simulations were smoothed with a Gaussian filter. This has two consequences. First, if we require the two filters to contain the same mass, then the scale associated with the tophat is about $R_{TH} \approx 1.6\, R_G$. In addition, we must account for the fact that the mean value of the overdensity in such a tophat is different from that in the Gaussian. If the distribution of the smoothed $\delta_{\rm G}$ and $\delta_{\rm TH}$ fields were Gaussian, then we could compute the average $\langle \delta_{\rm TH}, R_{\rm TH}|\delta_G, R_G\rangle$. This exercise shows that the mean value of the tophat fluctuation is typically larger (smaller) than that of the Gaussian in over (under) dense regions. This suggests that to compare with theory, we should use $R_{\rm TH} = 16$ Mpc/h, and the associated value of the overdensity. Using $\langle 1+\delta_{\rm TH}\rangle = 3.5$, and 0.4 for the two cases provides rms values which are similar to those

of the simulation. These values in our model give the solid curves in the two panels. The figures show that our model describes the differences between the two regimes quite well.

Including the fact that halo speeds depend on their environment (haloes in dense regions move faster than they do in underdense regions) was essential to reproduce the simulation results: whereas the dependence on density of the halo mass function (equation 3) controls the tails of the distribution, it is the dependence of halo speeds on density (equation 13) which controls the width of the central core. Neglecting this dependence produces distributions which have narrower/broader cores than those measured in the dense/underdense regions. Section 3 discusses why halo speeds depend on local density.

2.4 Dark matter haloes

Our model can also be used to estimate what happens to the shape of $f(v)$ if something other than dark matter particles are used as trace particles. For example, suppose we wish to construct the distribution of velocities if only haloes within some mass range are used. This was done by Croft & Efstathiou (1994). They found essentially no dependence of $\sigma_{\rm halo}$ on cluster mass for the massive clusters in their simulations. They also reported that, in the tails, the distribution of massive cluster velocities differed from a Maxwellian. Our model provides a simple explanation for their findings.

In our model, the distribution of halo speeds is given by equation (1), but now each halo contributes only once, so the weighting by mass should be removed (both from the numerator and the denominator). Also there should be no contribution from the $v_{\rm vir}$ term: so $p(v|m,\delta)$ is a Maxwellian (a Gaussian in one-dimension) with dispersion equal to the second term, $\sigma^2_{\rm halo}(m,\delta)$, in equation (14). If the range in halo masses and environments considered is sufficiently small, then $f(v)$ will be approximately Gaussian; departures from the Gaussian shape will become increasingly apparent as the range in m and δ is increased. Since $\sigma_{\rm halo}$ depends only weakly on halo mass (Figs. 1 and 2; note that this is consistent with Croft & Efstathiou) any departures from Gaussianity are almost entirely due to the dependence of halo speeds on δ.

As we show in the next section, the halo speeds do depend on δ. We were able to neglect this dependence when studying the speeds of dark matter particles, because the large velocity non-Gaussian tails were determined almost entirely by the virial motions of the particles, and not by the halo speeds. Since these virial motions do not contribute to the motions of the haloes themselves, they do not mask the effect of the density dependence of halo speeds on the distribution of $v_{\rm halo}$. Thus, in our model, both for the dark matter, and for the haloes, the distribution of speeds is predicted to have a non-Gaussian tail which is a consequence of adding up Gaussian distributions having different dispersions. However, whereas for the dark matter, this tail arises more from the mass dependence of the virial motions within dark haloes than from any dependence on environment, the tail in the distribution of halo speeds arises more from the fact that the halo speeds depend on environment than on halo mass.

To illustrate this, panels on the left of Fig. 7 show the distribution of halo speeds we obtained after splitting the

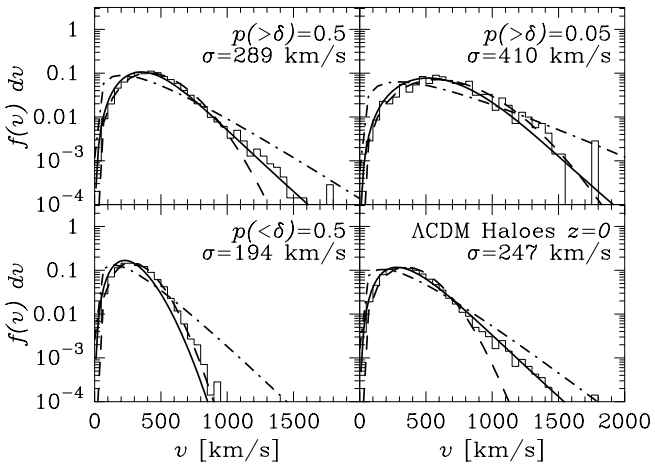

Figure 7. Dependence of the distribution of halo speeds on environment. Top left panel shows the distribution of three-dimensional speeds for 50% of the haloes, chosen because the local density around them is high, and bottom left panel shows the distribution for the other half. Top right panel shows the distribution when only 5% of the haloes, having the highest local density, are used. Bottom right panel shows the distribution of speeds for the total halo sample; it is quite different from a Maxwellian (dashed curve). Dot-dashed curve shows the corresponding Expwellian distribution associated with exponential one-dimensional distributions. Solid curves show what our model predicts.

total halo population into two samples, each containing half of the total sample, based on the value of the local density around each halo. The top left panel shows the distribution for the haloes in the dense regions, and the bottom left panel shows the distribution for the haloes around which the local density is smaller. The local density of a halo was computed by smoothing the dark matter field onto a 256^3 grid using a Gaussian filter of scale $R_G = 10$ Mpc/h, as described in the previous subsection. The local density of a halo was then set equal to the density of the nearest grid point.

For comparison, we also show two other distributions: a Maxwellian, and an 'Expwellian'. Whereas a Maxwellian has independent Gaussian variates for each of the three cartesian components of the velocity, the Expwellian has components which are exponentially distributed. The Maxwellian has the form

$$f_{\rm MB}(v,\sigma) = -2v\,\frac{\partial}{\partial v}\,\frac{{\rm e}^{-(v/\sigma)^2/2}}{\sqrt{2\pi\sigma^2}}, \qquad (15)$$

where σ is the rms of each of the components, whereas the Expwellian is

$$f_{\rm Exp}(v,\sigma) = -2v\,\frac{\partial}{\partial v}\,\frac{{\rm e}^{-\sqrt{2}(v/\sigma)}}{\sqrt{2\sigma^2}}. \qquad (16)$$

This way of writing the three-dimensional distributions follows from the assumption that the vector is drawn in a random direction and its length is independent of its direction; this in turn implies that its components have identical one-dimensional distributions (Feller 1966).

It would appear that the true distribution (histograms) is Maxwellian (dashed curves) in the less dense regions, but more 'Expwellian' (dot-dashed curves) if the local density is higher. This is consistent with our model (solid curves), because the range of δ is much smaller in the underdense than

the overdense regions. To illustrate that the non-Gaussian tail really does arise from mixing Maxwellian distributions with different dispersions, and not from velocities which are intrinsically non-Gaussian, the top right panel shows the distribution of speeds computed using haloes in the denser regions, but now with the cut at 5% rather than 50% of the total sample. In this case, even though the average value of the local density is considerably larger, the range of overdensities is smaller, and so our model predicts that the distribution should be well fit by a Maxwellian (with a larger dispersion, of course). The figure shows that this prediction is correct: even in these densest regions, where the haloes are moving significantly faster than in the rest of the simulation box, the components of the velocity are approximately Gaussian distributed.

The figure shows results for the full three-dimensional distributions; we did this because the one-dimensional distributions look quite Gaussian even when the range in δ is large. At first, this may seem unexpected: one usually thinks of the three-dimensional distribution as a sum of independent one-dimensional distributions, so if each component is Gaussian, then the full three-dimensional distribution should be Maxwellian. The reason why this does not happen is that the large v non-Maxwellian tail comes from Gaussians which have large dispersions. If the dispersion is large, then all three components are likelier to be large, so the three-dimensional speed is that much more likely to be large. Since the final distribution we are considering here is a sum over Gaussians of different dispersions, the difference between the three-dimensional distribution and a Maxwellian appears to be larger than the difference between each of the components and a Gaussian. Another way of saying this is that the departures from a Gaussian distribution are significant when $f(v) \leq 10^{-4}$, whereas the departures from Maxwellian are significant when $f(v)$ is an order of magnitude or so larger. In effect, this means that it takes fewer haloes to measure this difference reliably if one uses the three-dimensional distribution rather than the one-dimensional one. An important consequence of this is the following. Suppose that only one component of the velocity was measured and found to be approximately, but not exactly, Gaussian. Then the discussion above cautions strongly against concluding that the three-dimensional velocities were drawn from a Gaussian random field.

2.5 On isotropy and correlated components

There is an interesting aspect of our model which we have not discussed. The Maxwell-Boltzmann distribution associated with linear gravitational instability theory and Gaussian initial density fluctuations has the special property that the three components of the velocity are independent Gaussians, and the resulting velocity field is isotropic. If the components are non-Gaussian, then isotropy requires that the components be correlated (e.g. Feller 1966). We will show this explicitly below for a few toy examples.

Consider what happens when the velocity is the sum of two rather than three components. We will study the distribution of the angle θ between the vector and the x-axis in two steps; we will derive the distribution $Q(\tau)$ of $\tau \equiv \tan\theta = v_y/v_x$ first, and we will then use the fact that $\mathrm{d}\tau/\mathrm{d}\theta = (1+\tau^2)$ to compute the distribution of θ itself. And, for simplicity, we will only study the distribution in θ in the regime where both v_x and v_y are positive. (Of course, the distribution in the other quadrants can be derived analogously.) If v_x and v_y are independent, but have the same distribution p, then

$$Q(\tau) = \int p(v_x)\, p(v_y = \tau v_x)\, v_x\, \mathrm{d}v_x. \qquad (17)$$

If p is Gaussian or exponential, then

$$\begin{aligned} Q_{\rm Gauss}(\tau) &= (2\pi)^{-1}\,(1+\tau^2)^{-1} \qquad \text{and} \\ Q_{\rm Exp}(\tau) &= (1/4)\,(1+\tau)^{-2}. \end{aligned} \qquad (18)$$

so that

$$\begin{aligned} q_{\rm G}(\theta) &= 1/2\pi \qquad \text{and} \\ q_{\rm Exp}(\theta) &= (1/4)\,(\sin\theta + \cos\theta)^{-2}. \end{aligned} \qquad (19)$$

Whereas the distribution of θ associated with independent Gaussians is uniform, the one associated with Exponentials is not; it has a minimum at $\pi/4$. To get a uniform distribution in θ, v_x and v_y cannot be independent if they are not Gaussian. Had we chosen p distributions which were less centrally peaked than a Gaussian (the exponential is more centrally peaked), we would have found q distributions which have maxima, rather than mimima, at $\pi/4$. E.g. a uniform distribution on the range $0 \leq v \leq V$ has $q(\theta) \propto \cos^{-2}\theta$ and $\sin^{-2}\theta$ for $0 \leq \theta < \pi/4$ and $\pi/4 \leq \theta < \pi/2$, respectively.

One consequence of this is that if one wishes to model the nonlinear velocity field, and one requires that the nonlinear field be isotropic, then one's model must have correlations between the components of the velocity. Building such a model is not easy; of course, perturbation theory may be helpful here. We were able to circumvent this problem by assuming that, for sufficiently small ranges in mass and environment, the velocities are, in fact, Gaussian. This allowed us to use all the nice features of the Gaussian to build our model relatively easily, without worrying about correlations between the different velocity components. In our model, the total velocity distribution is built up by summing over many different Gaussian distributions. Since each of these is isotropic, the final field is also. Because the final distribution is non-Gaussian, but isotropic, the resulting distribution must have correlations between x, y and z components of the velocity built in, even though we never explicitly worried about how to model them correctly.

We have measured these correlations in the simulations using Spearman's rank correlation ρ for the three pairwise permutations of v_x, v_y, and v_z for the total halo population (those in the bottom right panel of Fig. 7). In all three cases we found values of about $\rho = 0.075$ with significance levels (which should lie between zero and one) of about 10^{-20}. These low values indicate that the correlation is extremely significant. The same test, with two independent normal variates for the components (same sample size of the halos $N = 14089$), yields $\rho = 0.0005$ and significance level 0.95, confirming that there is no correlation in this case. We then repeated this test using only those halos in the densest, and the least dense regions. Recall that our model assumes that, for a sufficiently small range in environment, the distribution should be Gaussian. In both these cases we find that this rank correlation statistic suggests that the velocity

components are independent and that therefore their distribution is, indeed, Gaussian.

2.6 Galaxies

Galaxies can also be treated within the context of our model, provided we assume that all galaxies form within dark matter haloes and that, for the most part, any given galaxy contains a small enough fraction of the mass of the parent halo that it can be thought of as a trace particle within the halo. This means that all we now need is a relation which tells us how, on average, the number of galaxies scales with halo mass. If $N_{\rm gal}(m)$ is known, then we can insert it in place of the factor of m in equation (1). This is clearly a very simple assumption, which we will discuss in more detail later. Note that this assumption can also be used to model how different the spatial distribution of galaxies is from that of the dark matter (Seljak 2000; Peacock & Smith 2000; Scoccimarro et al. 2000). First, we consider the shape of $N_{\rm gal}(m)$.

One might have thought that, on average, the number of galaxies in a halo would be proportional to the available gas, and that the fraction of gas should be proportional to the total mass of the parent halo: $N_{\rm gal}(m) \propto m$. However, because gas must cool to form stars, and the internal velocity dispersions of haloes increase with halo mass (cf. equation 7), gas cools less efficiently in more massive haloes. So, since the number of galaxies actually depends on the fraction of gas that can cool, $N_{\rm gal}(m) \propto m^{\mu}$, with $\mu < 1$, is more reasonable. In addition, there is a lower mass cutoff to this weighting scheme, which is associated with the fact that if the potential well of a halo is not sufficiently deep, the supernovae formed from the first generation of stars may blow the remaining gas out of the halo, thus supressing future star formation.

The fact that $N_{\rm gal}(m)$ depends on m has an important consequence for our model. If there are many galaxies in a halo, then it is reasonable to treat each one as a test particle, so that its velocity is similar to that of a dark matter particle. However, mass conservation means that a significant fraction of low mass haloes may have at most one galaxy within them. In such haloes, it makes more sense to identify the motion of the galaxy with that of the halo. Even in haloes which contain more than one galaxy, there is often one dominant central galaxy. It seems sensible to identify the motion of this galaxy with that of the parent halo, so that for this galaxy also, the virial term does not contribute. To model this, we will assume that both the virial and halo terms contribute to $N_{\rm gal}-1$ of the galaxies within a halo, but that only the halo term contributes for the final remaining galaxy.

Although this $N_{\rm gal}(m)$ weighting scheme for incorporating galaxies into our model is extremely simple, we think it provides a useful framework for constructing more complicated, and presumably more realistic, schemes. For example, it is known that ellipticals occur preferentially in clusters, whereas spirals occur in the field. Also, within a cluster, ellipticals are more strongly concentrated towards the cluster centre than are the spirals. The first fact can be incorporated into our scheme simply by using two different weighting schemes: $N_{\rm Ell}(m)$ and $N_{\rm Spiral}(m)$. If ellipticals populate more massive haloes, then, since the contribution of massive haloes to the peculiar velocity statistic is dominated by the virial term which increases with halo mass, one would expect the velocity dispersion of ellipticals to be larger than spirals.

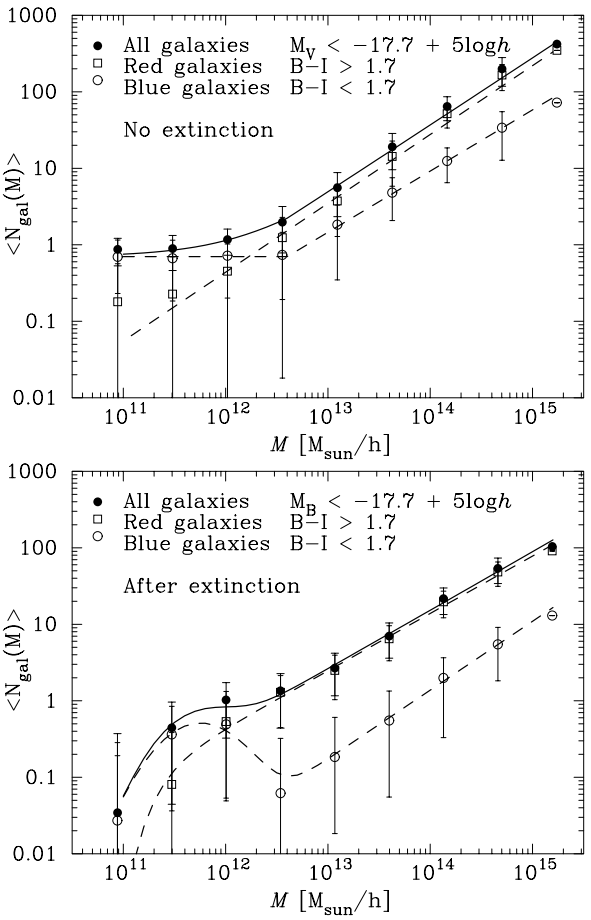

Figure 8. The average number of bright galaxies as a function of parent halo mass in the ΛCDM semi-analytic models of Kauffmann et al. (1999). Top panel shows results for a catalog in which no correction for the effects of dust was made. Bottom panel shows the galaxy catalog after correcting for extinction. Open circles show blue galaxies, open squares show red galaxies, and solid circles show the sum of the two populations. Curves show the simple fits to these relations discussed in the text.

The fact that ellipticals are concentrated more strongly towards cluster centres than spirals is slightly more complicated to incorporate. If we continue to assume that the galaxies trace the dark matter within the halo, then the assumption that all haloes are isothermal spheres means that we needn't make any change other than to the weighting term. That is to say, because the velocity dispersion is independent of position within the isothermal sphere, particles that are nearer the centre of the halo move similarly to those that are further away. Since, in fact, halo density profiles are more complicated than isothermal spheres, the velocity dispersions within the halo are actually functions of position, it may be that ellipticals and spirals actually have different $p(v|m)$ relations as well. This would, of course, complicate the relation between $\sigma_{\rm Ell}$ and $\sigma_{\rm Spiral}$, though it is likely that, in general, $\sigma_{\rm Ell} \geq \sigma_{\rm Spiral}$.

To illustrate how all this works, we will compare our model with results from the semi-analytic galaxy formation

models of Kauffmann et al. (1999). These models provide the $N_{\rm gal}(m)$ relations we need for our model. Extinction due to dust changes the brightness and colours of the model galaxies, so that the $N_{\rm gal}(m)$ relation we need depends on whether or not this effect has been account for. For this reason we have chosen to study two samples, and they are presented in the two panels of Fig. 8. The top panel shows galaxies brighter than $M_V = -17.7 + 5\log h$ in a model in which the effects of dust have been neglected, and the bottom panel shows the $N_{\rm gal}(m)$ relation for galaxies brighter than $M_B = -17.7 + 5\log h$ after accounting for extinction. In each panel, the filled circles show all galaxies brighter than the magnitude cut. The total population can be split into a blue sample (open circles) and a red sample (open squares); these are the objects which are classified as having colours with $B - I < 1.7$ and $B - I \geq 1.7$, respectively.

In what follows, we will use simple approximations (the curves in the Figure) to the semi-analytic results. For the galaxies in the top panel,

$$\begin{aligned} N_{\rm Blue}(m) &= 0.7 \qquad\quad \text{if } 10^{11}\,M_\odot/h \leq m \leq M_{\rm Blue} \\ &= 0.7\,(m/M_{\rm Blue})^{\alpha_B} \qquad \text{if } m > M_{\rm Blue} \\ N_{\rm Red}(m) &= (m/M_{\rm Red})^{\alpha_R} \qquad m \geq 10^{11}\,M_\odot/h \\ N_{\rm gal}(m) &= N_{\rm Blue}(m) + N_{\rm Red}(m), \end{aligned} \tag{20}$$

where $M_{\rm Blue} = 4\times10^{12}\,M_\odot/h$, $\alpha_{\rm B} = 0.8$, $M_{\rm Red} = 2.5\times10^{12}\,M_\odot/h$, and $\alpha_{\rm R} = 0.9$. Extinction due to dust changes the brightness and colours of the model galaxies. So we have also studied a sample which contains galaxies brighter than $M_B = -17.7 + 5\log h$, after accounting for the effects of dust. In this case, we find that

$$\begin{aligned} N_{\rm Blue}(m) &= (m/M_{\rm Blue})^{\alpha_B} + 0.5\,{\rm e}^{-4[\log_{10}(m/10^{11.75})]^2} \\ N_{\rm Red}(m) &= (m/M_{\rm Red})^{\alpha_R}\,{\rm e}^{-(2\times10^{11}/m)^2} \\ N_{\rm gal}(m) &= N_{\rm Blue}(m) + N_{\rm Red}(m), \end{aligned} \tag{21}$$

where $M_{\rm Blue} = 7\times10^{13}\,M_\odot/h$, $\alpha_{\rm B} = 0.9$, $M_{\rm Red} = 3\times10^{12}\,M_\odot/h$, and $\alpha_{\rm R} = 0.75$.

There are two reasons why one might worry that the semi-analytic models underestimate the number of bright galaxies in low-mass haloes. The first is that the models only resolve halos with $M > 1.4\times10^{11}\,M_\odot/h$. Secondly, the semi-analytics include a model for dynamical friction which may be more efficient than accurate numerical simulations suggest (Springel, White, Tormen & Kauffmann 2000). As a result, galaxies within a halo may merge with the central galaxy faster than they should, and so fewer (or just one) bright galaxies survive. On the other hand, in small mass haloes there simply isn't enough material available to make a massive satellite object in addition to the central galaxy, so having a small number of bright galaxies in low-mass haloes is certainly sensible.

Whatever the reason for this low mass cutoff, our main purpose here is to show how our model for the dark matter $f(v)$ distribution can be extended to describe galaxies. Thus, although the low mass cutoff in the $N_{\rm gal}(m)$ relation may not be in exactly the right place, our main interest is in the fact that this cutoff occurs in different places for the blue than the red galaxies. This has quite dramatic consequences on the predicted $f(v)$ distribution.

When Kauffmann et al. (1999) identify galaxies in the simulations, each halo with at least one galaxy is assigned a central galaxy. The velocity of this central galaxy is chosen to be the same as that of the dark matter particle which has the greatest absolute value of the potential energy. In the real universe, the central galaxy is plausibly almost at rest with respect to the barycentre of its dark matter halo, whereas in the simulations the central galaxy moves, on average, with a velocity of $\sim$ 80 km/s with respect to the barycenter of its dark halo. Therefore, we used the mean velocity of the dark particles of the parent halo for the velocity of the central galaxy. The histograms in Fig. 9 show the resulting distribution of bright galaxy peculiar velocities in the extinction-corrected simulations (those in the bottom panel of Fig. 8). Results for the simulations in which no dust correction was applied are sufficiently similar that we decided against showing them here.

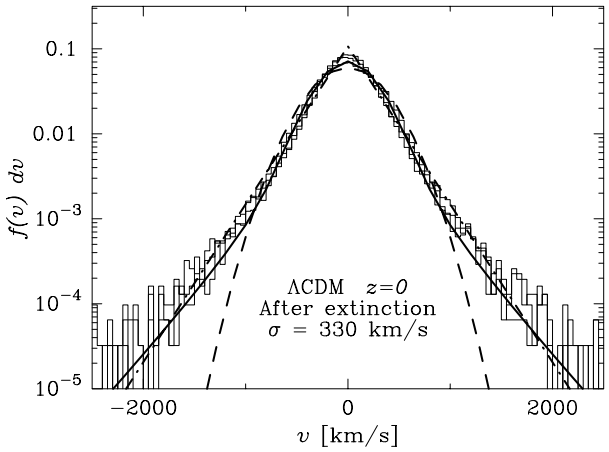

Figure 9. Distribution of peculiar velocities of model galaxies which, after correcting for the effects of dust, are brighter than $M_B = -17.7 + 5\log h$. Histograms show results from the ΛCDM models of Kauffmann et al. (1999). Dashed and dot-dashed curves show Gaussian and exponential distributions which have the same dispersion. Solid curve shows the distribution predicted by our $N_{\rm gal}(m)$ models (lower panel of previous figure).

Notice that although $f_{\rm gal}(v)$ has a slightly different shape than the dark matter statistic, it still has tails which are significantly different from a Gaussian. Dashed and dot-dashed curves still show Gaussian and exponential distributions which have the same dispersion. The solid curve shows what our simple $N_{\rm gal}(m)$ model predicts—it provides a good description of the simulation results.

Fig. 10 shows how the semi-analytic and our model $f(v)$ distributions depend on galaxy type. Notice that the red galaxies have larger dispersions than the blue, as expected if they occur predominantly in more massive haloes. We have chosen to present these results using linear plots because peculiar velocity catalogs currently available contain on the order of a few thousand galaxies, rather than the 10^5 or so in the simulations. In practice, the errors on each peculiar velocity measurement are likely to be on the order of a few hundred km/s. These will broaden the curves somewhat, making the difference between the red and blue samples less dramatic.

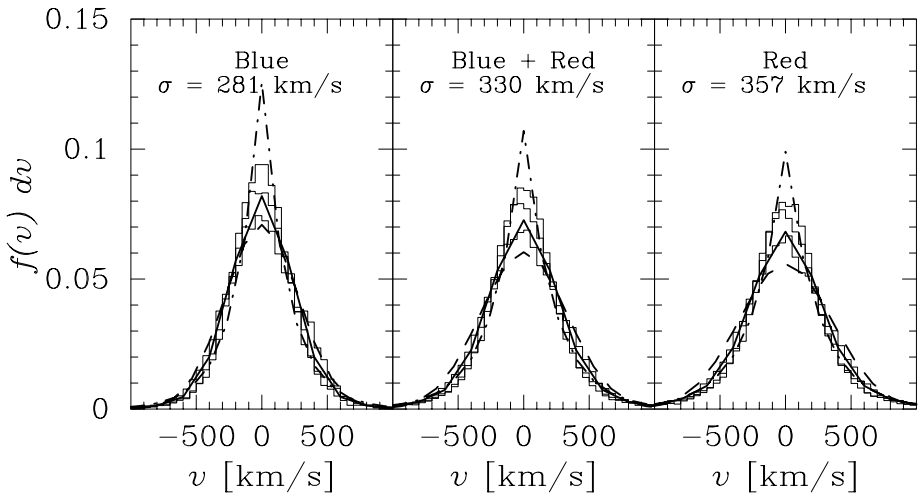

Figure 10. Distribution of peculiar velocities of model galaxies as a function of colour; colours were assigned after accounting for the effects of dust. The panels on the left and right show blue and red galaxies, and the one in the middle shows the sum of the two. Line-styles are as in previous figure.

3 THE EVOLUTION OF HALO VELOCITIES

This section is motivated by the results of Colberg et al. (2000) who reported that linear theory underestimates the evolution of the speeds of massive haloes. This underestimate is more severe when massive halos have near neighbours. This section argues that, indeed, the evolution of halo speeds, and so the accuracy of linear theory, depends not so much on halo mass as on local density.

The previous section showed (Figs. 1 and 2) that combining linear theory with the assumption that haloes at $z = 0$ may be associated with peaks in the initial conditions provides a reasonably good description of the speeds of haloes at $z = 0$. The lower set of symbols in the panels on the right of Figs. 1 and 2 show the halo velocities in the simulation at $z = 20$. Following Colberg et al (2000), a halo's velocity at $z = 20$ is computed using the same particles that are in it at $z = 0$, but using the velocities they had at $z = 20$, rather than the velocities they actually have at $z = 0$. The lower dashed curve in the panel on the right was computed using equation (8) at $z = 20$, assuming that there was no power in modes with $k \leq 2\pi/L$. This means that the lower dashed curve differs from the upper one by the linear theory velocity growth factor ($\propto \sqrt{a}$ in SCDM); on a log plot the two dashed curves have the same shape. (Although there is a slight offset—the theory curve should be multiplied by about 0.9 if it is to pass through the $z = 20$ symbols—it has the same shape as the symbols. Though they do not remark on it, a comparison of columns 9 and 17 in Table 2 of Colberg et al. 2000 shows the same offset.)

Although the dashed curves appear to have the same shape as the symbols, both at $z = 20$ and at $z = 0$, there is a systematic discrepancy: the model appears to underestimate the amount by which the speeds of massive haloes have evolved. This discrepancy is the same as that reported by Colberg et al. (2000). At face value, this suggests that the accuracy of the linear theory evolution of halo speeds depends on halo mass. In fact, we will argue that the actual evolution depends not so much on halo mass as on local density. It is well known that the evolution of clustering within dense regions is accelerated relative to the average (e.g. Tormen & Bertschinger 1996; Cole 1997)—we show that this applies to the evolution of halo speeds also. In particular, we argue that the evolution of halo speeds is best estimated by using an $\Omega_{\rm eff}$ which depends on (some suitably defined) local density, rather than the global value Ω_0. We describe a simple model in which massive haloes populate denser regions, so that the dependence on density appears as a dependence on halo mass.

After studying the accuracy of the predicted linear theory amplitude, this section turns to the direction of motion predicted by linear theory. It shows that nonlinear kicks to a particle's motion may substantially change the particle's direction. Although the amplitude of the nonlinear kicks are larger for particles which end up in massive haloes, these kicks are random in direction, so they can be estimated easily. The directions of halo motions, on the other hand, are extremely well described by linear theory. That is to say, haloes identified at any given time are moving in essentially the same direction as predicted by linear theory. This provides additional justification for our model in which nonlinear effects are modelled as arising primarily from virial motions within haloes.

3.1 Massive haloes populate denser regions

Suppose one assumes that massive haloes form near peaks in the initial fluctuation field, and that they are close to local minima in the initial potential field (Kaiser 1984; Bardeen et al. 1986). Colberg et al. (2000) show this is true for the most massive objects present at $z = 0$. In such a model, less massive haloes fall towards the massive ones, so one might expect the speeds of less massive haloes to be higher in regions which contain massive haloes. This leads to the question: Do massive haloes populate denser regions than average?

Equation (3) for $n(m|\delta)$ suggests that massive haloes occur predominantly in denser cells (recall that for massive haloes $b(m)$ increases with m). Although this is intuitively

obvious—one reason a cell is denser is because it contains massive objects—the Appendix provides a simple quantitative model of the average density of cells which are known to contain haloes of a given mass m. Therefore, in a model in which less massive haloes stream towards the more massive ones, one might expect the speeds of less massive haloes to be higher in denser regions than in less dense ones. Moreover, since the evolution of clustering is accelerated in dense regions relative to the average, one might expect halo speeds to also evolve faster in dense regions than in underdense regions.

In such a model, massive haloes populate dense regions, so the evolution of their speeds is best estimated by using an $\Omega_{\rm eff}$ which is larger than the global value. Moreover, massive haloes which have massive near neighbours are, on average, in even denser regions. Since $\Omega_{\rm eff}$ is even larger for the massive haloes which have massive neighbours, one might expect the discrepancy with the linear theory evolution to be even larger for such haloes than for those which are relatively isolated. This is qualitatively consistent with what Colberg et al. (2000) found in their simulations: the discrepancy between the linear theory predicted velocity at $z = 0$ and the actual velocity of a halo at that time is larger for massive haloes which have massive neighbours nearby.

This argument applies to less massive haloes also, although in this case things are complicated by the fact that less massive haloes occupy regions spanning a wider range of densities—their speeds evolve faster or slower than average depending on whether or not they are in denser or less dense regions. On average, however, less massive haloes occupy regions of about average density, and so using the global value of Ω_0 to estimate the evolution of the population as a whole will be reasonably accurate. This is why using the global value of Ω_0 to extrapolate from $z = 20$ to $z = 0$ works well for less massive haloes, but results in an underestimate of the present day velocities of massive haloes.

How does such a model compare with what happens in simulations?

3.2 Comparison with simulations: speed

Fig. 11 shows the velocities of haloes at $z = 0$ as a function of the 'local' density at that time. The local density was computed by smoothing the density field at $z = 0$ with a Gaussian filter of radius $R_G = 4{\rm Mpc}/h$. In the top two and bottom left panels, the bins in the x-direction were chosen to contain equal numbers of haloes, the error bars show the range containing 90 percent of the haloes in the bin, and the symbols show the median velocity and density for each bin. The three panels show haloes of different mass ranges. In all three panels, there is a clear trend for haloes in dense regions to move faster. Also, comparison of the three panels shows that, on average, massive haloes populate denser cells. The bottom right panel shows this trend with halo mass more clearly. The open squares, filled squares, open circles and filled circles show the median velocities of haloes, and the median densities of the cells populated by haloes containing 60-100, 10^2-10^3, 10^3-10^4 and 10^4-10^5 particles, respectively (the same symbols and ranges as in Fig. 2). The error bars show the range in which 90% of the haloes in the given mass ranges lie (though we have not done so here, we could have estimated these ranges directly from the work of Sheth & Lemson 1999). At $z = 0$, massive haloes clearly populate denser regions, and they clearly move slightly slower than less massive haloes.

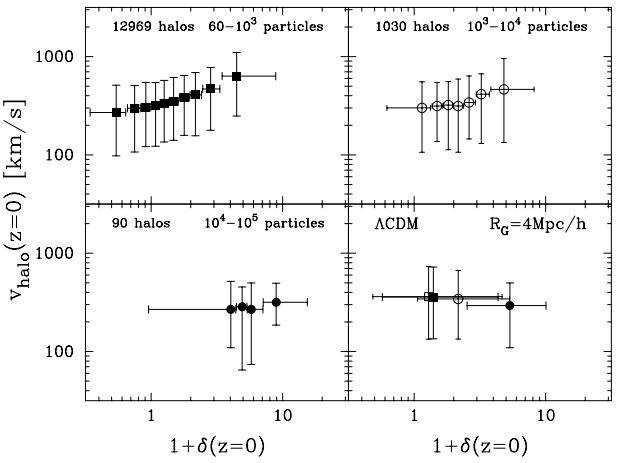

Figure 11. Dependence of halo speed at $z = 0$ on local density at $z = 0$ for haloes of different masses. Haloes in dense regions are moving faster than haloes in underdense regions. On average, massive haloes populate denser regions, and move slightly more slowly than less massive haloes. This is consistent with a model in which massive haloes are associated with minima in the initial potential field, and less massive haloes are falling towards these minima.

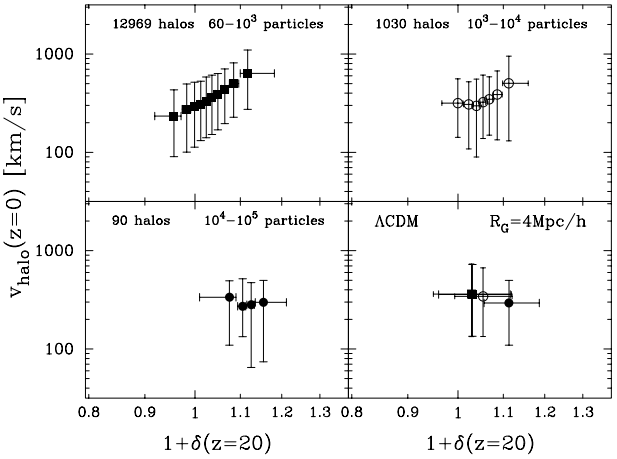

Figure 12. Dependence of halo speed at $z = 0$ on local density at $z = 20$, for haloes of different masses. At the present time haloes which were initially in dense regions are moving faster than haloes which were initially in underdense regions. This trend is true for haloes of all masses.

We have also constructed such a plot using $R_G = 10{\rm Mpc}/h$. On this larger smoothing scale also, the trend for higher halo speeds in denser cells at $z = 0$ remains: $v \propto (1+\delta)^\alpha$ with $\alpha \geq 0$. Although α increases with R_G because the range in densities is smaller at large R_G, whereas the halo velocities do not depend on R_G, most of this difference in slope can be accounted for as follows.

On average, dense cells at $z = 0$ were also dense initially. The spherical collapse model allows us to estimate the initial overdensity δ_0 given the density $1 + \delta$ today (Mo & White 1996 provide a simple fitting formula for this relation). If

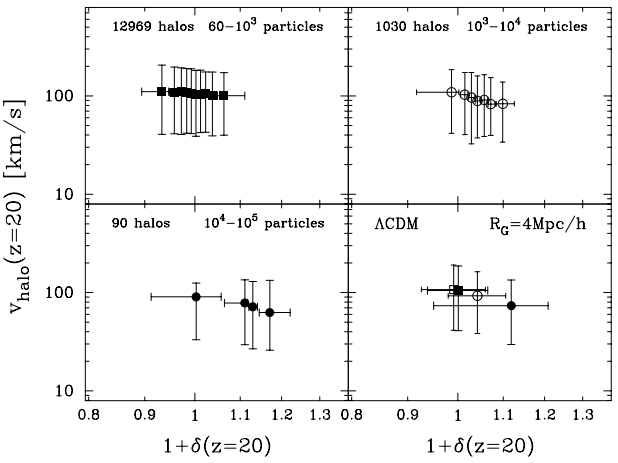

Figure 13. Dependence of halo speed at $z = 20$ on local density at $z = 20$, for haloes of different masses. Except for a weak trend for haloes in dense regions to move more slowly (the trend is reversed at $z = 0$ anyway), there is little correlation between halo speed and surrounding density. This suggests that the tendency to move faster in denser regions, shown in the previous figure, must be due to evolution.

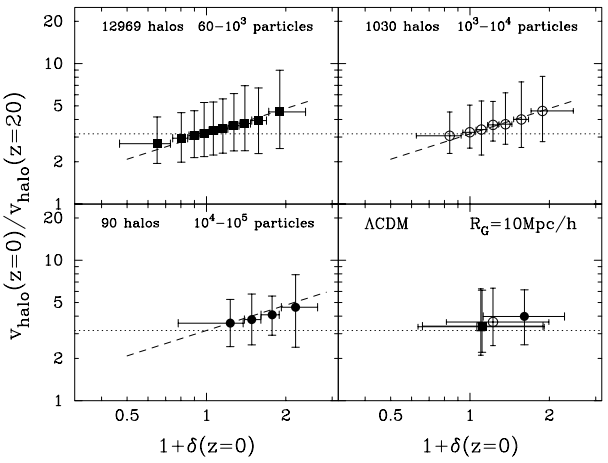

Figure 14. Dependence of the ratio of the halo speeds at $z = 0$ and $z = 20$ on local density at $z = 0$, for haloes of different masses. Dotted lines in each panel show the linear theory prediction; dashed lines, the same in each panel, show equation (22). The measured ratio is higher in denser regions; velocities in dense regions evolve faster than in less dense regions. The dependence on density is approximately the same for all haloes—it does not depend on halo mass.

we were to rescale the x-axes to show the initial δ_0, rather than the density today, then this would move the bins with $\delta > 0$ to the left, and the bins with $\delta \leq 0$ to the right. The magnitude of the shift would be larger for large values of $|\delta|$. As a result, the plot for $R_G = 10\mathrm{Mpc}/h$ would remain essentially unchanged (this just says that large regions have not changed their size very much since the initial conditions, and $\delta_0 \approx \delta$ for small δ) whereas the plot for $R_G = 4\mathrm{Mpc}/h$ would change significantly. If we were to apply this rescaling, then $v \propto [1+\delta_0(\delta)]^\alpha$, with the nearly the same value of α for a range of smoothing scales: $4 \leq R_G \leq 10\mathrm{Mpc}/h$. Of course, once the smoothing scale on which δ is defined becomes very large, the trend with 'local' density vanishes. This scale is approximately the same as that on which the mass function of haloes approaches the global value: $n(m|\delta) \to n(m)[1 + b(m)\delta]$, but $\delta \ll 1$.

Rather than apply this spherical collapse $\delta_0(\delta)$ rescaling, we have done the following. We have taken all the particles that are in a halo at $z = 0$, found their positions at $z = 20$, and plotted $v_{\rm halo}(z = 0)$ versus $1 + \delta$ at $z = 20$. Fig. 12 shows this when the smoothing scale used to define the 'local' density at $z = 20$ was $R_G = 4\mathrm{Mpc}/h$. Notice the correlation between higher speeds and local densities. This figure should be compared with Fig. 13 in which the local densities were computed using $R_G = 4\mathrm{Mpc}/h$ at $z = 20$ but the halo velocities were computed using the velocities the particles had at $z = 20$. The difference between the two plots is striking. Notice that, for all but the most massive haloes, the velocities at $z = 20$ show no dependence on the local density at that time. Because a sphere of size $R_G = 4\mathrm{Mpc}/h$ in which the overdensity is δ at $z = 0$ was actually larger at $z = 20$ [by a factor of $(1 + \delta)^{1/3}$], it is not really fair to compare plots in which the same smoothing scale is used for both times. We have found no dependence of $v_{\rm halo}(z = 20)$ on local density at $z = 20$ even when the density is computed by smoothing with larger filters. (At $R_G = 20\mathrm{Mpc}/h$, there is a weak trend for the halo speeds to be smaller in denser cells, even for the less massive haloes. It would be interesting to know if this were real. Though we have not done so, it should be possible to do the linear theory calculation for the predicted bulk motion of a region subject to the condition that the region of interest is embedded in a larger scale over/underdensity. For the special case in which the scales on which the initial velocities and densities are smoothed are the same, linear theory predicts no dependence of the initial velocities on the initial densities, which is approximately what our bottom panel shows.) We interpret the fact that halo velocities at $z = 20$ are independent of local density at $z = 20$, but halo velocities at $z = 0$ do depend on local density at $z = 20$ as strong evidence that the evolution of halo velocities depends on their environment.

To quantify this, Fig.14 shows the ratio of the median halo velocity at $z = 0$, v_0 to that at $z = 20$, v_{20}, as a function of local density at $z = 0$, computed using $R_G = 10\mathrm{Mpc}/h$. For the ΛCDM model studied here, the linear theory prediction is that $v_0/v_{20} = 3.16$; it is shown as the horizontal dotted curve in the panels. The different symbols in each bin show the different mass ranges. This shows that the evolution of halo velocities depends more on environment than on halo mass. The dashed curves show

$$\frac{v_0}{v_{20}} = (1+\delta)^{\mu(R)}\, f_{\rm lt}, \qquad (22)$$

where $f_{\rm lt} \propto \Omega_0^{0.6}$ is the growth factor predicted by linear theory, and $\mu(R = 10\,\mathrm{Mpc}/h) = 0.6$. The dashed curves in the three panels all show this same scaling—the dependence of halo speed on local density is independent of halo mass. The trend in the bottom right panel of Fig.14 only reflects the fact that massive halos are in denser regions.

As discussed earlier, $\mu(R)$ depends on the scale R on which the local density field was defined. A reasonable approximation to the dependence on R can be got by setting $\mu = 0.6\,\sigma^2(R)/\sigma^2(10\,\mathrm{Mpc}/h)$, where $\sigma^2(R)$ denotes the variance in the present day density field when smoothed on scale

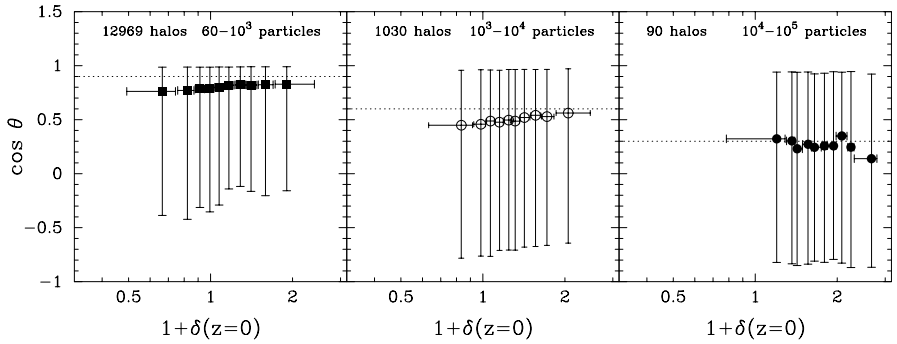

Figure 15. The dot product of the linear and actual directions of motion for dark matter particles in less massive (left), intermediate (middle) and massive (right) halos, as a function of overdensity. Symbols show the median and error bars show the range containing 90% of the particles in each bin. The nonlinear kicks to a particle's motion are larger in massive halos. Dashed line shows the expected median if kicks are randomly distributed.

R. Alternatively, as discussed earlier, one might have chosen to incorporate the dependence on R by using $[1+\delta_0(\delta)]$ instead. The main point we wish to make is that our simple fit, equation (22), strongly suggests that the dependence of the evolution of halo speeds on local density can be very simply parametrized by replacing the global value of Ω_0 with what is, effectively, a local one.

Because the rms speeds of halos depend on environment, one might have wondered if the full distribution of halo speeds, rather than just the rms, depends on environment. However, as we showed in the previous section (Fig. 7), if one studies a sufficiently small range of halo masses and environments, then $p(v_{\rm halo}|m,\delta)$ is Gaussian/Maxwellian, to a good approximation. When the range in m and δ is increased, the distribution develops a non-Gaussian large v tail; this happens not because the velocities themselves are non-Gaussian, but because, when one considers a wide range in δ, one sees the effect of summing up Gaussians which have a wide range of widths.

3.3 Comparison with simulations: direction

In addition to a speed, linear theory also predicts a direction of motion. This subsection shows that the linear theory direction does not provide a good indicator of the direction of motion of dark matter particles at $z=0$. It is, nevertheless, a very good indicator of the direction of halo motions. Essentially, this is because the motion of a dark matter particle receives substantial nonlinear kicks as it becomes part of a virialized halo—the amplitude of the nonlinear kicks increases with halo mass. Haloes themselves do not suffer substantial kicks to their motion.

In what follows, we will interpret the difference $v_0 - v_{20}$ as the nonlinear kick to a particle's motion. Fig. 15 shows

$$\cos\theta = \frac{v_0 \cdot v_{20}}{|v_0||v_{20}|} \qquad (23)$$

as a function of local density for the dark matter particles for a range of halo masses. The figure clearly shows that the nonlinear kicks to a particle's motion are larger in massive haloes. If these kicks were randomly distributed in direction, then the present day direction would be the sum of two independent Gaussian vectors having different, but known, dispersions, $\sigma^2_{\rm halo}(m)$ and $\sigma^2_{\rm vir}(m)$, which can estimated from the results of the previous section (Fig. 2). This allows us to compute the distribution of $\cos\theta$. For random kicks the mean value should be

$$\langle\cos\theta\rangle = \frac{1}{\sqrt{1+\sigma^2_{\rm vir}(m)/\sigma^2_{\rm halo}(m)}}. \qquad (24)$$

(This follows from the fact that if the kicks are random, then the initial direction of motion and the direction of the kick are, on average, at right angles to each other.) For the range of halo masses in the three panels above, this would require $\langle\cos\theta\rangle \approx 0.9$, 0.6 and 0.3, which is in reasonable agreement with the Figure.

Fig. 16 shows the corresponding distribution for the halo motions. Although the nonlinear kicks to a halo's motion are larger in denser regions, these kicks are almost always smaller than the initial velocity.

Fig. 17 presents one consequence of the fact that the nonlinear kicks to a halo's motion are larger in denser regions. The figure shows that the deflection $\theta_{\rm halo}$ is large both at small and large values of v_0/v_{20}. Because large values of v_0/v_{20} are associated with dense regions (Fig. 14), the large range in $\theta_{\rm halo}$ at large v_0/v_{20} is, perhaps expected. The reason this happens at small v_0/v_{20} as well is slightly more subtle. There is a hint associated with the fact that the magnitude of the scatter is the same in the smallest and largest bins, and it is approximately the same as the scatter in the largest density bin in Fig. 16. Presumably, the haloes with small $\cos\theta_{\rm halo}$ and small v_0/v_{20} are precisely the ones which scatter low in the densest cells in Fig. 14; these are the haloes in dense regions which have suffered large kicks to their initial velocities, so they are now travelling in quite different directions than they were initially. Of course, because these are the haloes in the densest bins, they are only a small fraction of the set of all haloes. Figs. 16 and 17 show that, for most haloes, the linear theory direction is a good indicator of the direction of motion today.

To summarize: This section makes two points. The first is that linear theory provides a good description of the initial speeds of haloes, but tends to underestimate the rate at which the speeds of massive haloes evolve. Although second-order perturbation theory is the best way to study why this happens, our results suggest that this happens because the evolution of halo speeds is faster in denser regions. The speeds of massive haloes evolve faster than linear

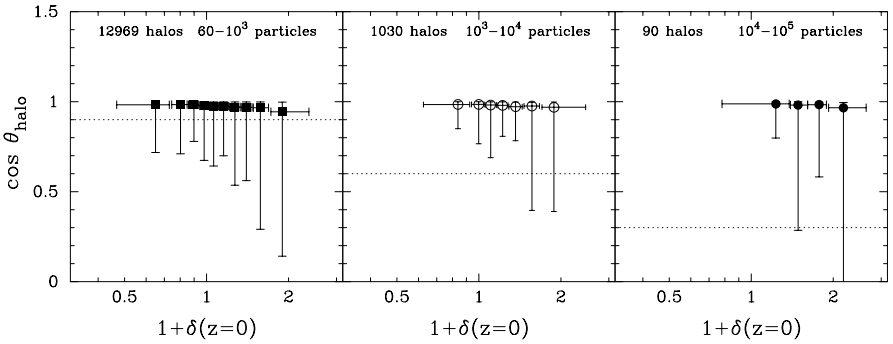

Figure 16. The dot product of the linear and actual directions of motion for less massive (left), intermediate (middle), and massive (right) halos, as a function of overdensity. Symbols show the median and error bars show the range containing 90% of the haloes in each bin. The nonlinear kicks to a halo's motion are small; they are larger in denser regions. Dotted lines (same as the previous figure) represent the typical kick received by a dark matter particle.

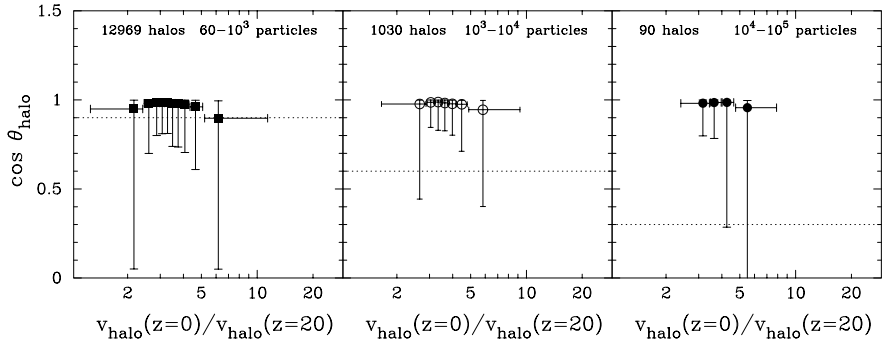

Figure 17. Relation between the direction of a halo's motion and the evolution of its speed. Panels show the dot product of the linear and actual directions of motion for less massive (left), intermediate (middle) and massive haloes (right) versus the ratio of the actual and initial, linear, speeds. The large scatter in directions at small and large v_0/v_{20} are from haloes in dense regions.

theory predicts primarily because they populate denser regions. Therefore, it may be sufficient to model the evolution of halo speeds by replacing the global value of the density parameter, Ω_0, in equation (8), with a local $\Omega_{\rm eff}$. Once this adjustment has been made, linear theory provides a good description of the distribution of halo speeds. In addition, linear theory provides a good description of the directions of halo motions. That is to say, once $\Omega_0 \to \Omega_{\rm eff}$, an approach based on the Zeldovich approximation should be reasonably accurate at describing halo motions. The same is not true, of course, for the motions of dark matter particles; particles receive substantial nonlinear kicks as they become incorporated into clusters. These kicks are approximately randomly distributed in direction.

3.4 Comparison with simulations: Virial motions

We have assumed throughout that the virial term depends on mass more strongly than it does on local density. For completeness, we think it useful to show that this is accurate.

The symbols with error bars in the four panels in Fig. 18 show $\sigma_{\rm vir}$ as a function of local density for ΛCDM haloes in four different mass ranges; least massive haloes are top left, and most massive haloes are bottom right. The mass cuts were chosen to be the same as in Fig. 2, so the symbols in this figure are the same as in that one. And as before, the error bars show the range in each bin within which 90% of the haloes are. The density was defined by smoothing the particle distribution on a grid with a Gaussian filter of width 4Mpc/h. The dotted curves show the value of $\sigma_{\rm vir}$ predicted by the virial theorem (our equation 7) for the associated mass range. The dotted curves were computed using the global value of the density parameter Ω_0, not the local one. They provide a reasonable fit to the simulations. For massive haloes (bottom panels), $\sigma_{\rm vir}$ appears to be higher in denser regions. This is almost entirely a consequence of the fact that the densest cells contain the more massive haloes in the mass bin. To illustrate this, we have computed the median halo mass in each density bin, using only the haloes in the requisite mass range for each panel, and used this mass to compute $\sigma_{\rm vir}$. These values are shown as the crosses in each panel—they have been offset downwards by a factor of 0.25 (i.e., the plot shows the virial velocity divided by $10^{0.25}$) for clarity. The crosses show the same trend as the main symbols, demonstrating that the virial term really does depend on mass, and not on local density.

4 DISCUSSION

We described a model in which galaxy velocities were written as the sum of two terms, one of which was effectively described using linear theory, and the other which was inherently nonlinear. We showed that this split was both useful

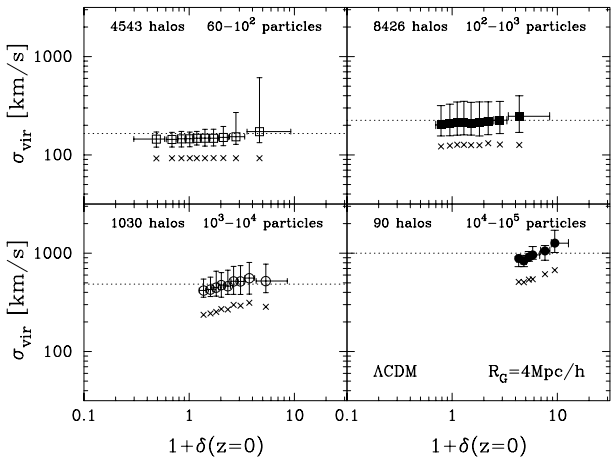

Figure 18. Dependence of virial motions on halo mass and local density in the ΛCDM simulations. Symbols in the top left panel show the lowest mass haloes, symbols in the bottom right panel show the most massive haloes. Dotted curve shows equation (7) computed for the median halo mass in the panel, and using Ω_0, the global, not the local, value of the density. Crosses (offset downwards for clarity) show the result of inserting the median mass in each bin into equation (7) to compute $\sigma_{\rm vir}$.

and accurate for clustering which develops from Gaussian initial conditions, although our model should also work for more general initial conditions. For Gaussian initial conditions, a generic prediction of our model is a Gaussian core, with exponential wings for the distribution of galaxy peculiar velocities. The core mainly reflects the fact that most dark matter haloes move with the same speed, and this speed is less than the virial motions within clusters (both these are consequences of the Gaussian initial conditions); the wings arise primarily from the large nonlinear virial velocities within massive clusters. We compared our model with one dimensional peculiar velocity distribution functions $f(v)\,{\rm d}v$ extracted from dissipationless N-body simulations, where galaxies were formed and evolved with semi-analytic techniques. Our model, which explicitly considers whether dark matter particles, galaxies or galaxy clusters trace the velocity field, accounts for the shape of $f(v)\,{\rm d}v$ extremely well.

We are not the first to have considered the shape of the galaxy distribution function statistic. Saslaw et al. (1990) present a formula for $f(v)\,{\rm d}v$ which is accurate for N-body simulations of clustering from Poisson initial conditions. The virtue of our approach is that it shows clearly how the distribution should depend on trace particle type. Raychaudhury & Saslaw (1996) present a measurement of $f(v)\,{\rm d}v$ using a sample of spirals compiled by Mathewson, Ford & Buchhorn (1992). It would be interesting to do the same with the more recent SFI and ENEAR data sets of spirals and ellipticals. Since our models depend explicitly on cosmology, it may be that these data sets are able to place interesting constraints on the density parameter.

Section 3 argued that halo speeds evolve faster in denser regions. The fact that massive haloes populate denser regions has consequences for estimates of Ω_0, studies of how and why the local value of the cosmic Mach number may differ from the global one, and the detection of the kinematic Sunyaev-Zeldovich effect.

Suppose one were to measure the peculiar velocities of galaxies. Since measuring distances is difficult, the velocity of any one galaxy is often ill-determined. To increase signal to noise, one often 'groups' galaxies, before using their 'grouped' velocities. If these groups correspond approximately to dark matter haloes, then this is useful, because we showed that linear theory describes the directions of halo motions rather well. However, one often then weights all subsequent analyses by the signal-to-noise ratio. In effect, this means that the signal-to-noise weighted grouped velocities are dominated by the motions of massive haloes. Since the motions of massive haloes evolve more quickly than average, they have a higher effective density parameter than the global value. It is interesting, therefore, that peculiar velocity based estimates of Ω_0 are often higher than those indicated by almost all other observations (e.g., Smith et al. 1999; Branchini et al. 2000; Zaroubi et al. 2000; but see Borgani et al. 2000).

The cosmic Mach number is the ratio of the large scale bulk velocity to the smaller scale velocity dispersion (Ostriker & Suto 1990). Recent work (van de Weygaert & Hoffman 1999) suggests that local measurements of this Mach number may differ from the global one. Because our model is also phrased in terms of bulk flows and dispersions, it can be used to address this issue analytically. For example, it allows one to study how the distribution of the Mach number statistic depends on local density.

An obvious consequence of our results is that large overdense regions, namely superclusters, are ideal places to look for the kinematic Sunyaev-Zeldovich effect: in these regions, low mass haloes, with relatively low optical depth, can have substantial peculiar velocities; they thus can yield detectable kinematic Sunyaev-Zeldovich fluctuations in the Cosmic Microwave Background radiation (Diaferio, Sunyaev and Nusser 2000). In this context, our model for the distribution of halo speeds, and its dependence on density, is then related to the distribution of temperature fluctuations one might measure.

Our results suggest that whereas nonlinear effects can be thought of as adding Gaussian noise to the initial linear theory velocity, this noise is higher for particles in massive haloes. Therefore, the noise is spatially dependent—adding or subtracting a global thermal noise before comparing observations with theory may lead to inconsistencies. Should one choose to use a global thermal noise anyway (e.g. Freudling et al. 1999), then the 'temperature' associated with ellipticals (e.g. the ENEAR catalog), which occur more in clusters, will be larger than that for spirals (e.g., the SFI catalog) which occur more in the field.

Our derivation of the single particle velocity distribution function is the first step in a larger program. Baker, Davis & Lin (2000), following Davis, Miller & White (1997), consider a statistic which is essentially a smoothed version of our $f(v)$ distribution. The operation of smoothing is essentially one of adding several, possibly correlated, velocities. So, to compute the smoothed statistic from our model requires knowledge of how the halo velocity correlation function depends on halo mass. We are in the process of extending our model to include the effects of smoothing.

Finally, our results suggest that, once account has been taken for the effect of the local density on the evolution of velocities, linear theory (or the Zeldovich approximation)

should provide a reasonably good estimate of the motions of haloes. This simplifies models of redshift-space distortions considerably (work in progress). Catelan et al. (1998) describe a dark-matter halo based model of the density field in which motions are approximated using the Zeldovich approximation. Our results suggest that if their approach were to be extended to describe redshift-space distortions, then it should be quite accurate.

ACKNOWLEDGMENTS

Thanks to Enzo Branchini, Mike Hudson, Mariangela Bernardi, Michael Blanton, Jörg Colberg, Lam Hui, Román Scoccimarro, Rien van de Weygaert, Saleem Zaroubi and Idit Zehavi for helping shape our thoughts on these subjects. The N-body simulations, halo and galaxy catalogues used in this paper are publically available at `http://www.mpa-garching.mpg.de/NumCos`. The simulations were carried out at the Computer Center of the Max-Planck Society in Garching and at the EPCC in Edinburgh, as part of the Virgo Consortium project. In addition, we would like to thank the Max-Planck Institut für Astrophysik where this project began, and where some of the computing for this work was done, and Simon White for prompting us to think about the question of isotropy. RKS is supported by the DOE and NASA grant NAG 5-7092 at Fermilab. He thanks the Department of Physics as well as the Observatory at Torino for their warm hospitality in May 2000.

REFERENCES

Baker J. E., Davis M., Lin H., 2000, ApJ, in press
Bardeen J.M., Bond J.R., Kaiser N., Szalay A., 1986, ApJ, 304, 15
Benson A. J., Baugh C. M., Cole S., Frenk C. S., Lacey C. G., 1999, MNRAS, submitted
Borgani S., Bernardi M., da Costa L. N., Wegner G., Alonso M. V., Willmer C. N. A., Pellegrini P. S., Maia M. A. G., 2000, ApJL, in press, astro-ph/0005450
Branchini E., Zehavi I., Plionis M., Dekel A., 2000, MNRAS, in press, astro-ph/9911046
Bryan G., Norman M., 1998, APJ, 495, 80
Catelan P., Lucchin F., Matarrese S., Porciani C., 1998, MNRAS, 297, 692
Colberg J. M., White S. D. M., MacFarland T. J., Jenkins A., Pearce F. R., Frenk C. S., Thomas P. A., Couchman H. M. P., 2000, MNRAS, 313, 229
Cole S., 1997, MNRAS, 286, 38
Croft R. A. C., Efstathiou G., 1994, MNRAS, 268, L23
da Costa L. N., Bernardi M., Alonso M. V., Wegner G., Willmer C. N. A., Pellegrini P. S., Rité G., Maia M. A. G., 2000, AJ, in press
Davis M., Miller A., White S. D. M., 1997, ApJ, 490, 63
Diaferio A., Geller M., 1996, ApJ, 467, 19
Diaferio A., Sunyaev R., Nusser A., 2000, ApJL, 533, 71
Feller W., An Introduction to Probability Theory and Its Application, Vol. II. J. Wiley & Sons, New York
Freudling W., Zehavi I., da Costa L. N., Dekel A., Eldar A., Giovanelli R., Haynes M. P., Salzer J. J., Wegner G., Zaroubi S., 1999, ApJ, 523, 1
Haynes M. P., Giovanelli R., Salzer J. J., Wegner G., Freudling W., da Costa L. N., Herter T., Vogt N. P., 1999a, AJ, 117, 1668
Haynes M. P., Giovanelli R., Chamaraux P., da Costa L. N., Freudling W., Salzer J. J., Wegner G., 1999b, AJ, 117, 2039
Kaiser N., 1984, ApJL, 284, L9
Kauffmann G., Colberg J. M., Diaferio A., White S. D. M., 1999, MNRAS, 303, 188
Kepner J. V., Summers F. J., Strauss M. A., 1997, New Astronomy, 2, 165
Lemson G., Kauffmann G., 1999, MNRAS, 302, 111
Lucchin F., Matarrese S., 1988, ApJ, 330, 535
Mathewson D. S., Ford V. L., Buchhorn M., 1992, ApJS, 81, 413
Mo H. J., White S. D. M., 1996, MNRAS, 282, 347
Ostriker J. P., Suto Y., 1990, ApJ, 348, 378
Peacock J., Smith R., 2000, MNRAS, submitted, astro-ph/0005010
Peebles P. J. E., 1980, The Large Scale Structure of the Universe. Princeton Univ. Press, Princeton
Press W., Schechter P., 1974, ApJ, 187, 425
Raychaudhury S., Saslaw W. C., 1996, ApJ, 461, 514
Saslaw W. C., Chitre S. M., Itoh M., Inagaki S., 1990, ApJ, 365, 419
Robinson J., Baker J., 2000, MNRAS, 311, 781
Scoccimarro R., Sheth R. K., Hui L., Jain B., 2000, ApJ, submitted
Seljak U., 2000, MNRAS, accepted, astro-ph/0001493
Sheth R. K., 1996, MNRAS, 279, 1310
Sheth R. K., Lemson G., 1998, MNRAS, 304, 767
Sheth R. K., Tormen G., 1999, MNRAS, 308, 119
Sheth R. K., 2000, MNRAS, submitted
Sheth R. K., Mo H., Tormen G., 2000, MNRAS, submitted
Smith R. J., Hudson M. J., Lucey J. R., Schlegel D. J., Davies R. L., 1999, in Proceedings of the Cosmic Flows Workshop, eds. S. Courteau, M. Strauss, and J. Willick
Springel V., White S. D. M., Tormen G., Kauffmann G., 2000, MNRAS, submitted
Tormen G., Bertschinger E., 1996, ApJ, 472, 14
van de Weygaert R., Hoffman Y., 1999, in Evolution of large scale structure: from recombination to Garching, Proceedings of the MPA-ESO cosmology conference, eds. A. J. Banday, R. K. Sheth and L. N. da Costa.
Willick J. A., Courteau S., Faber S. M., Burstein D., Dekel A., Strauss M. A., 1997, ApJS, 109, 333
Zaroubi S., Bernardi M., da Costa L. N., Hoffman Y., Alonso M. V., Wegner G., Willmer C. N. A., Pellegrini P. S., 2000, MNRAS, submitted, astro-ph/0005558

APPENDIX A: THE DENSITY IN CELLS CONTAINING HALOES

Massive haloes populate denser cells: this Appendix provides a simple estimate of how the mean density in cells which contain at least one halo of mass m increases as m increases.

Let $p(\delta)\,\mathrm{d}\delta$ denote the probability that a cell of size V has overdensity in the range $\mathrm{d}\delta$ about δ, and let $p(j|\delta)$ denote the probability that such a region in which the overdensity is δ contains j haloes of mass m. The mean overdensity within cells of size V which contain at least one halo of mass m is

$$\Big\langle \delta | \text{at least one halo} \Big\rangle = \frac{\int \mathrm{d}\delta\ \delta\, p(\delta)\ [1-p(j=0|\delta)]}{\int \mathrm{d}\delta\ p(\delta)\ [1-p(j=0|\delta)]},$$

where the denominator is the fraction of cells that contain at least one halo of mass m.

If $p(j|\delta)$ were Poisson, then the probability that $j=0$ would be $\mathrm{e}^{-n(m|\delta)V}$. Sheth & Lemson (1999) show that this is a reasonable assumption on large scales. Since there are

many more low-mass haloes than massive ones, this exponential term tends to zero for small masses, and so the integrals above reduce to $\langle\delta\rangle = 0$. This says that the average overdensity in cells containing at least one less massive halo is zero. Massive haloes are slightly more complicated. To see how the integrals scale, it is useful to consider the large scale limit. In this limit, the linear bias model is reasonably accurate: $n(m|\delta) \approx n(m)\,[1 + b(m)\delta]$, where $b(m)$, the linear bias factor, increases as the mass m of the haloes of interest increases. To simplify things even further, suppose that $n(m|\delta)V \ll 1$ (although this assumption is inconsistent with the assumptions of linear bias and Poisson statistics, it helps illustrate our argument more clearly). Then $1 - p(j = 0|\delta) \approx n(m)V\,[1 + b(m)\delta]$ and the integrals above become

$$\Big\langle \delta|\text{at least one halo}\Big\rangle = \frac{\big\langle \delta\, n(m)V\,[1 + b(m)\delta]\big\rangle}{\big\langle n(m)V\,[1 + b(m)\delta]\big\rangle} = b(m)\,\big\langle\delta^2\big\rangle,$$

where we have used the fact that $\langle\delta\rangle \equiv 0$. Since $b(m)$ increases as m increases, this says that at fixed V, the mean density of cells in which there is at least one halo of mass m increases as m increases. This is in qualitative agreement with Fig. 11 which shows that the median density of cells which contain at least one halo of mass m increases as m increases.